Supporting Information

3D Confinement Zinc Plating/Stripping with High Discharge Depth and Excellent High-Rate Reversibility

Yurong Zhou,[ab†] Xiaona Wang,[a†] Xiaofan Shen,[b] Yanhong Shi,[a] Chengfeng Zhu,[a] Sha Zeng,[a] Hao Xu,[a] Pei Cao,[a] Yulian Wang,[a] Jiangtao Di,*[ac] and Qingwen Li*[ac]

[a]Key Laboratory of Multifunctional Nanomaterials and Smart Systems, Advanced Materials Division, Suzhou Institute of Nano-Tech and Nano-Bionics, Chinese Academy of Sciences, Suzhou 215123, China.

[b]Nano Science and Technology Institute, Suzhou 215123, China

[c]Division of Nanomaterials, Suzhou Institute of Nano-Tech and Nano-Bionics, Chinese Academy of Sciences, Nanchang 330200, China

* Corresponding author.

† These authors contributed equally to this work.

Email: jtdi2009@sinano.ac.cn (J. Di); qwli2007@sinano.ac.cn (Q. Li)

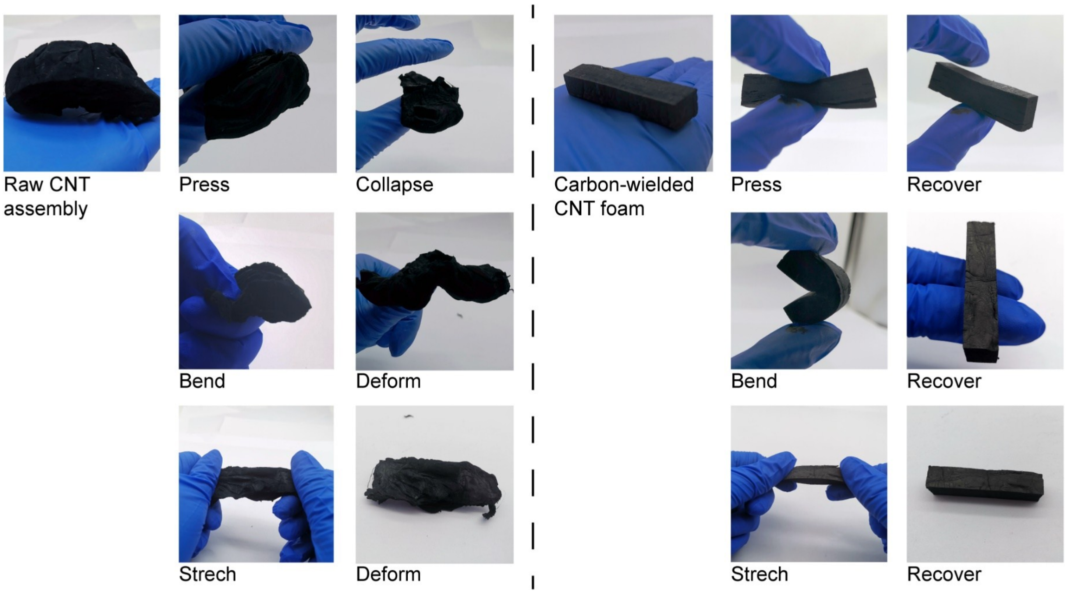

Figure S1. Comparison between the raw CNT foam (left column) and the carbon-wielded CNT foam (right column) when subjected to compression, stretch, and bending. The deposited carbon can stabilize the 3D structure of CNT foam by avoiding the slippage between CNTs or CNT bundles. Therefore, the carbon-wielded CNT foam can bear mechanical compression, bending, and stretching without structure collapse.

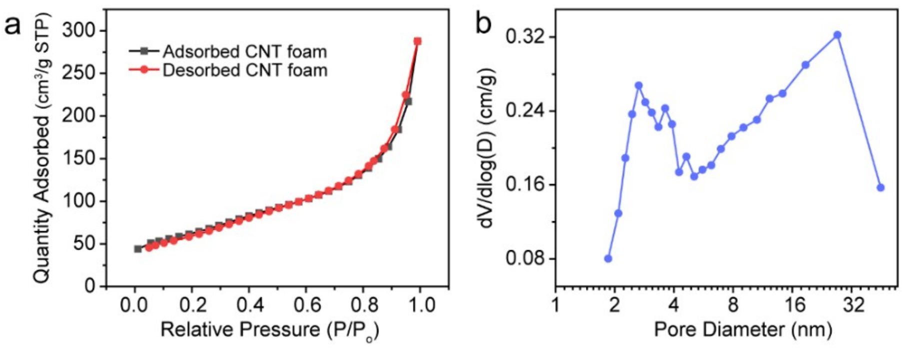

Figure S2. a) The BET surface area (about 221.1 m^2 g^{-1}) and b) the average pore diameter (about 8.05 nm) of CNT foam.

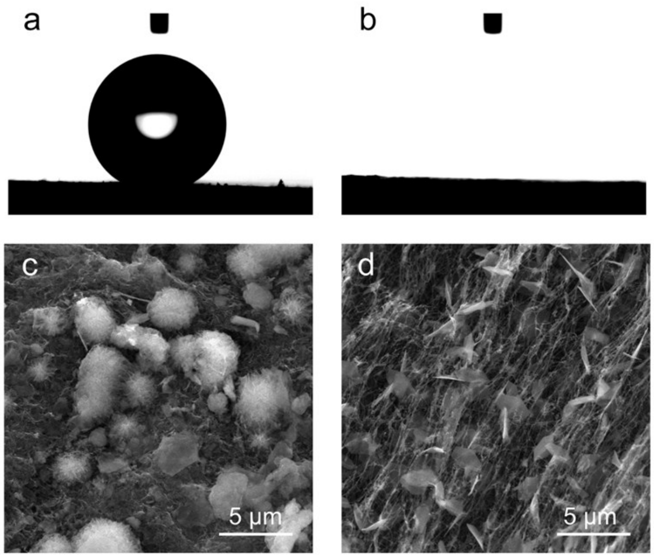

Figure S3. The contact angle measurement of water droplets on a carbon-wielded CNT foam a) before and b) after electrochemical treatment. The treated CNT foam became hydrophilic (soaked water droplet). SEM images of c) zinc particles on the surface of the carbon-wielded CNT foam without electrochemical treatment and d) uniform zinc deposition on the foam after electrochemical treatment. We did not observe the deposition of zinc inside of the foam that was not electrochemically treated. The comparison results indicate that the hydrophilic surface caused by electrochemical treatment can facilitate the electrolyte infiltration and the zinc plating and stripping within the 3D CNT network.

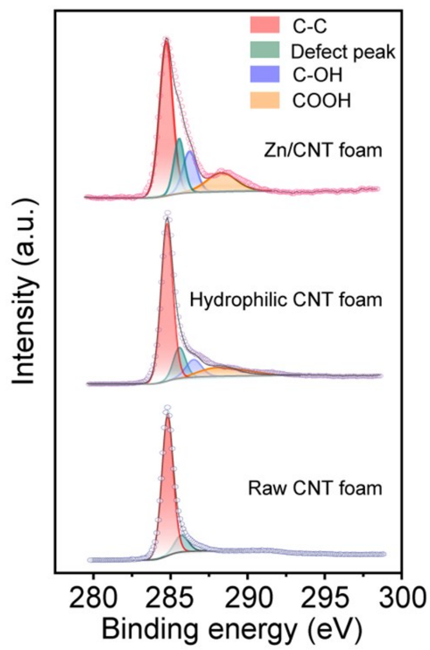

Figure S4. XPS data of the raw Zn/CNT foam, hydrophilic CNT foam and Zn/CNT foam. Hollow circles correspond to the experimental data.

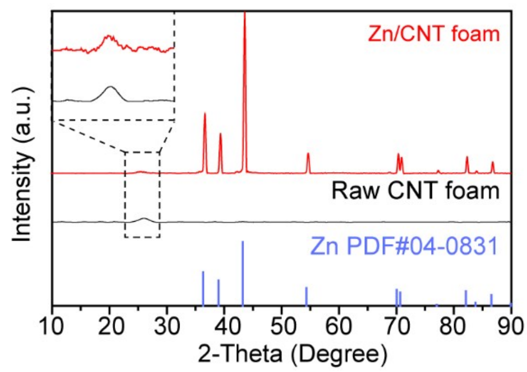

Figure S5. XRD data of Zn/CNT foam and raw CNT foam.

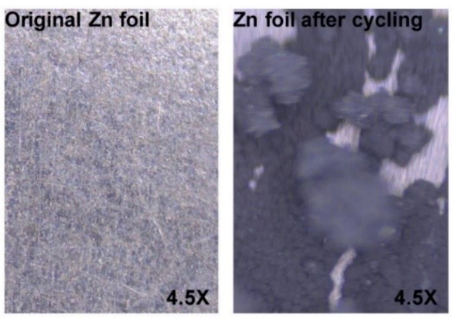

Figure S6. The change of macro-morphology of the Zn foil after cycling.

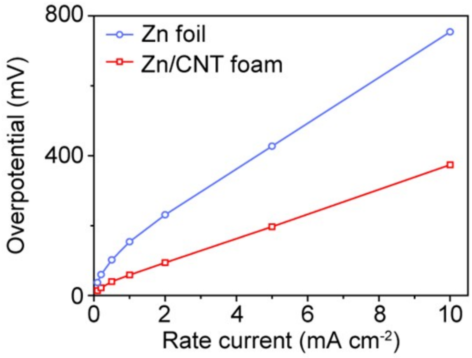

Figure S7. Overpotentials at different rate currents of symmetrical Zn cells with Zn foils and Zn/CNT foams.

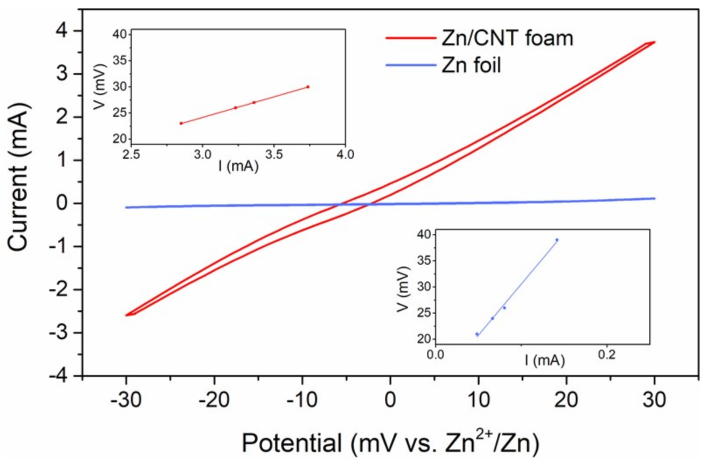

Figure S8. CV curves of Zn foil and Zn/CNT foam at 1 mV s^{-1} using a three-electrode configuration: the Zn/CNT foam or the Zn foil as the working electrodes, a Zn metal reference electrode, and a Pt counter electrode. Insert shows the V-I slop of two electrodes.

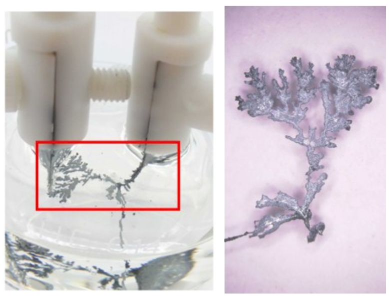

Figure S9. The digital photos of dendrite-induced short-circuiting after 50 cycles at 40% DOD_{Zn}.

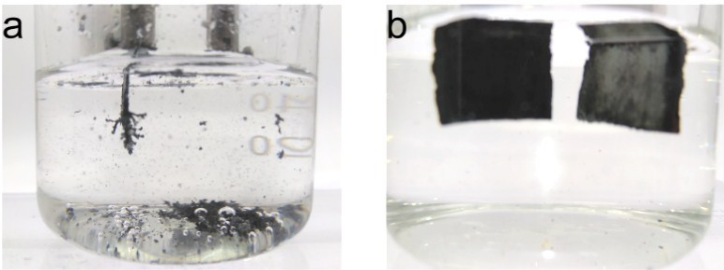

Figure S10. Digital photos of a) dead Zn exfoliation on Zn foils and b) highly reversible Zn/CNT foam electrodes.

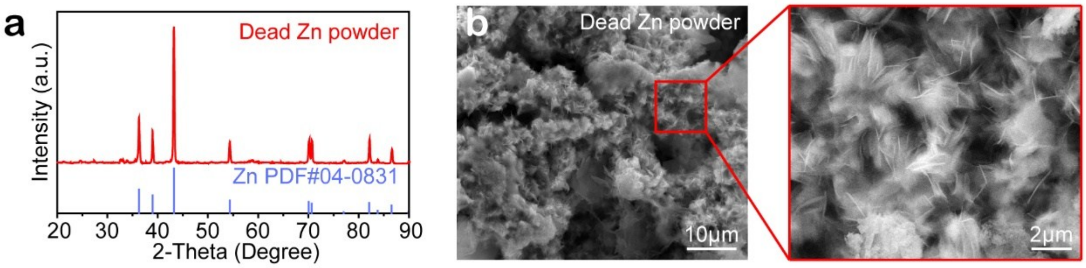

Figure S11. a) XRD spectrum and b) SEM images of dead Zn.

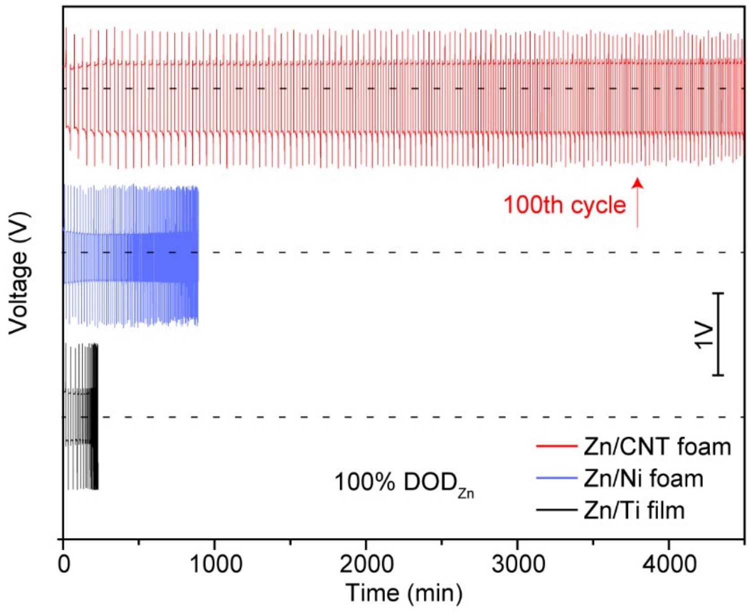

Figure S12. Galvanostatic cycling of symmetrical Zn cells with Zn/CNT foam (red), Zn/Ni foam (blue) and Zn/Ti film (black) during full charge-discharge cycling corresponding to 100% DOD$_{Zn}$. Scale bar: 1 V. Zn was electrodeposited by one pulse current electrodeposition process for the same time on different substrates, and a constant current density of 20 mA cm^{-2} and a cut-off voltage of 0.9 V are set for cycling.

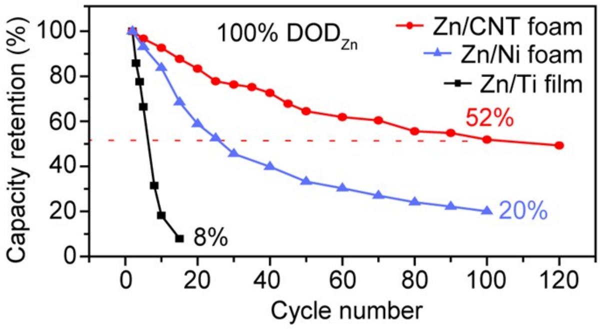

Figure S13. Capacity retention as a function of cycling number for symmetrical cells using Zn/Ti films (black), Zn/CNT foams (red), and Zn/Ni foams (blue). The DOD_{Zn} is 100% for these cells.

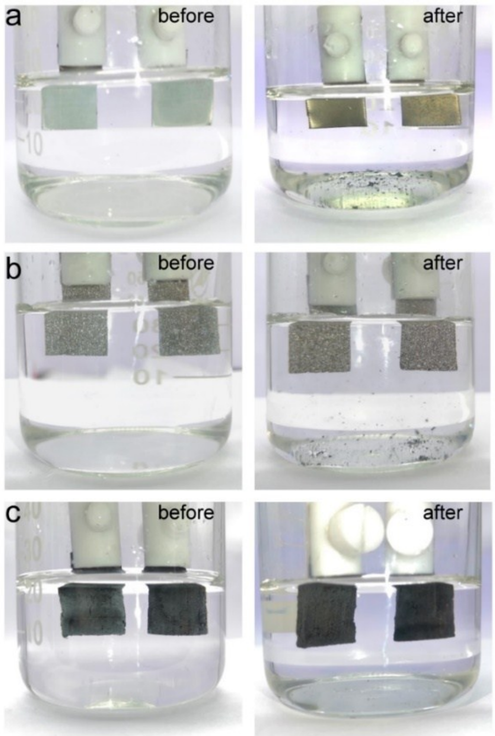

Figure S14. Digital photos of a) Zn/Ti film and b) Zn/Ni foam c) Zn/CNT foam before and after cycling at 100% DOD_{Zn}.

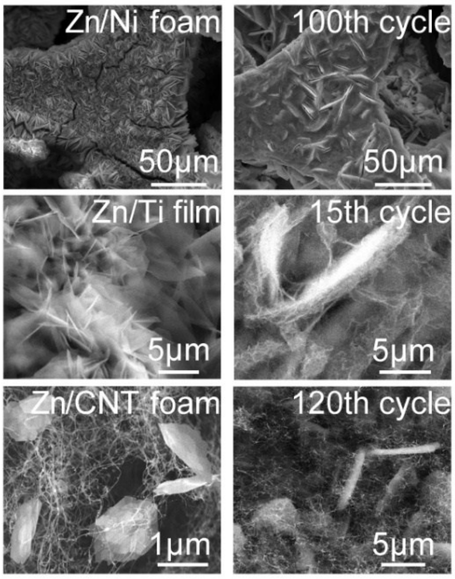

Figure S15. SEM images of the Zn/CNT foam, Zn/Ni foam and Zn/Ti film symmetrical cells before and after 100% DOD_{Zn} cycling.

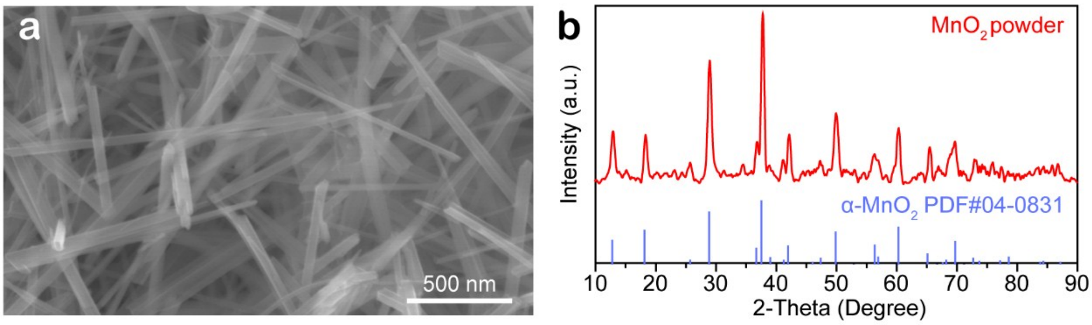

Figure S16. SEM images of (a) α-MnO_2 powder, and (b) its XRD spectra.

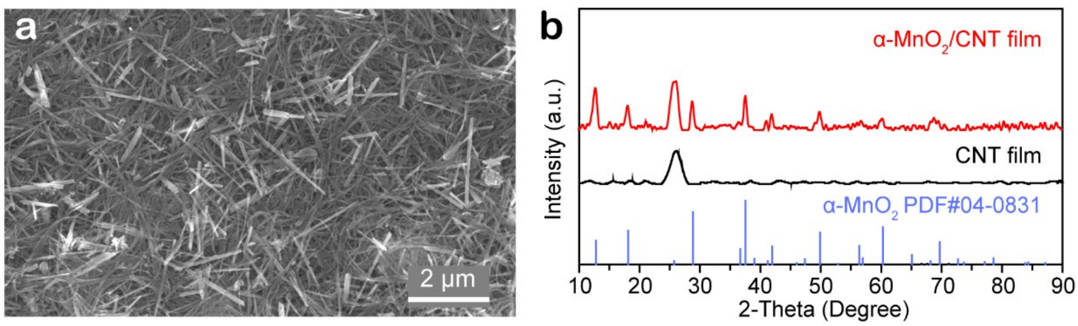

Figure S17. (a) SEM images of α-MnO_2/CNT film and (b) XRD spectra.

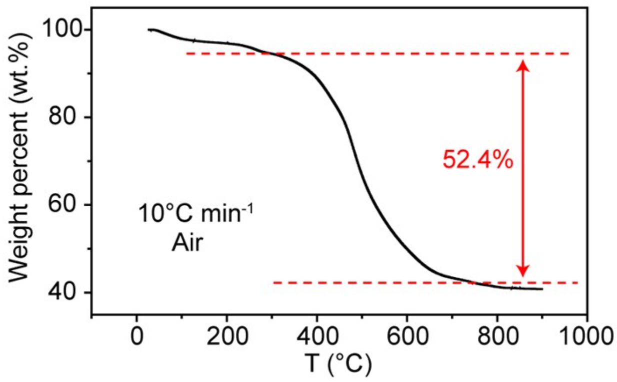

Figure S18. TAG curve of MnO_2/CNT film cathode.

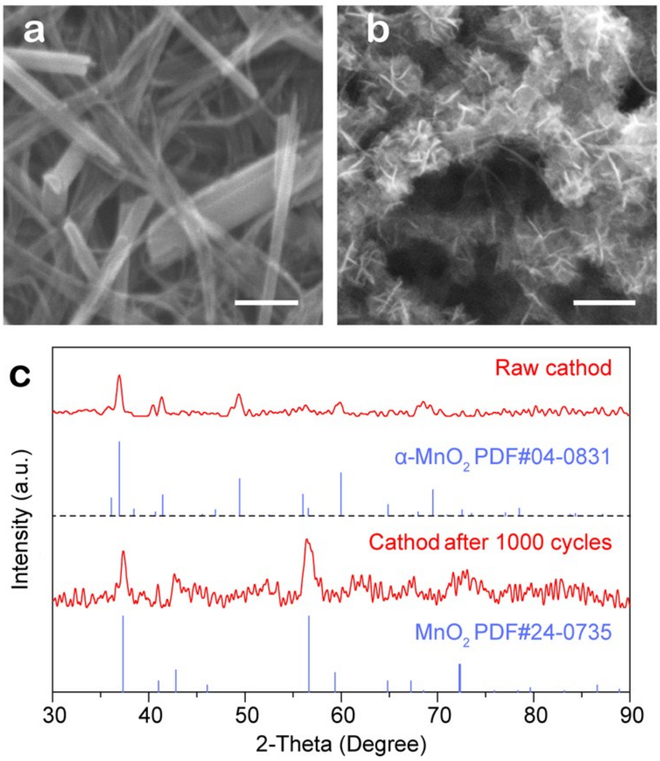

Fig. S19 The SEM images of MnO_2/CNT cathode a) before charge and discharge (scale bar: 200 nm), b) after 1000 cycles (scale bar: 200 nm), c) the XRD spectra of the MnO_2/CNT cathode before cycles and after 1000 cycles.

Figure S20. A timer driven by a quasi-solid flexible Zn/CNT foam//MnO_2/CNT film battery.

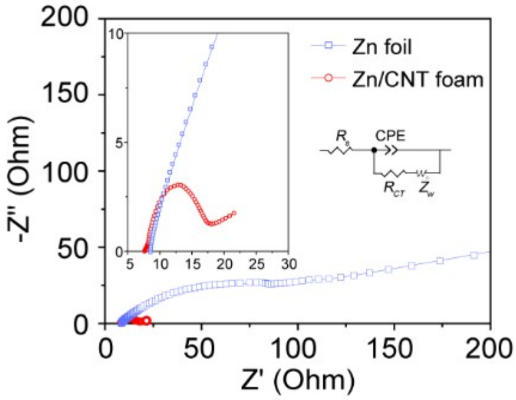

Figure S21. ESI curves of symmetrical Zn cells with Zn foil and Zn/CNT foam.

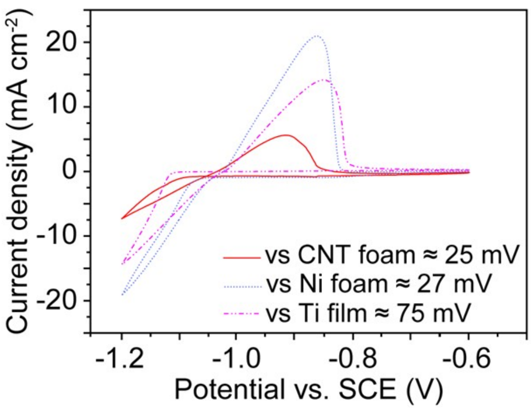

Figure S22. CVs for Zn plating/stripping on CNT foam, Ni foam and Ti film at 5 mV s^{-1}.

Table S1. Comparison of cathode capacities between literature results and our batteries.

Number	Capacities at low rates (mAh g^{-1})	Capacities at high rates (mAh g^{-1})	Materials	Ref.
(1)	224 (1C)	76 (10C)	PA based coated Zn foil	1
(2)	206 (1 A g^{-1})		nano-$CaCO_3$-coated Zn	2
(3)	260.4 (0.2 A g^{-1})	117 (1.5 A g^{-1})	Zn/CNT yarn	3
(4)	265.1 (0.2 A g^{-1})	20.3 (2 A g^{-1})	single-atomic layer MnO_2 nanosheets	4
(5)	210 (0.2 A g^{-1})	114 (2 A g^{-1})	oxygen Defects in β-MnO_2	5
(6)	220 (1C)	138 (20C)	δ-MnO_2 and $TFSI^-$ based electrolyte	6
(7)	250 (0.2 A g^{-1})	110 (2 A g^{-1})	Zn@ZnO-3D	7
(8)	260 (1C)	110 (10C)	α-MnO_2	8
(9)	272 (1C)	198 (10C) 82 (30C)	Zn/CNT foam	This work

Reference：

1. Z. Zhao, J. Zhao, Z. Hu, J. Li, J. Li, Y. Zhang, C. Wang and G. Cui, *Energy Environ. Sci.*, 2019, **12**, 1938-1949.
2. L. Kang, M. Cui, F. Jiang, Y. Gao, H. Luo, J. Liu, W. Liang and C. Zhi, *Adv. Energy Mater.*, 2018, **8**, 1801090.
3. H. Li, Z. Liu, G. Liang, Y. Huang, Y. Huang, M. Zhu, Z. Pei, Q. Xue, Z. Tang, Y. Wang, B. Li and C. Zhi, *ACS Nano*, 2018, **12**, 3140-3148.
4. W. Qiu, Y. Li, A. You, Z. Zhang, G. Li, X. Lu and Y. Tong, *J. Mater. Chem. A*, 2017, **5**, 14838-14846.
5. M. Han, J. Huang, S. Liang, L. Shan, X. Xie, Z. Yi, Y. Wang, S. Guo and J. Zhou, *iScience*, 2020, **23**, 100797.
6. Y. Jin, L. Zou, L. Liu, M. H. Engelhard, R. L. Patel, Z. Nie, K. S. Han, Y. Shao, C. Wang, J. Zhu, H. Pan and J. Liu, *Adv. Mater.*, 2019, **31**, 1900567.
7. X. Xie, S. Liang, J. Gao, S. Guo, J. Guo, C. Wang, G. Xu, X. Wu, G. Chen and J. Zhou, *Energy Environ. Sci.*, 2020, **13**, 503-510.
8. N. Zhang, F. Cheng, J. Liu, L. Wang, X. Long, X. Liu, F. Li and J. Chen, *Nat. Commun.*, 2017, **8**, 405.